Article

Cell Reports

Osteocyte-Intrinsic TGF-β Signaling Regulates Bone Quality through Perilacunar/Canalicular Remodeling

Graphical Abstract

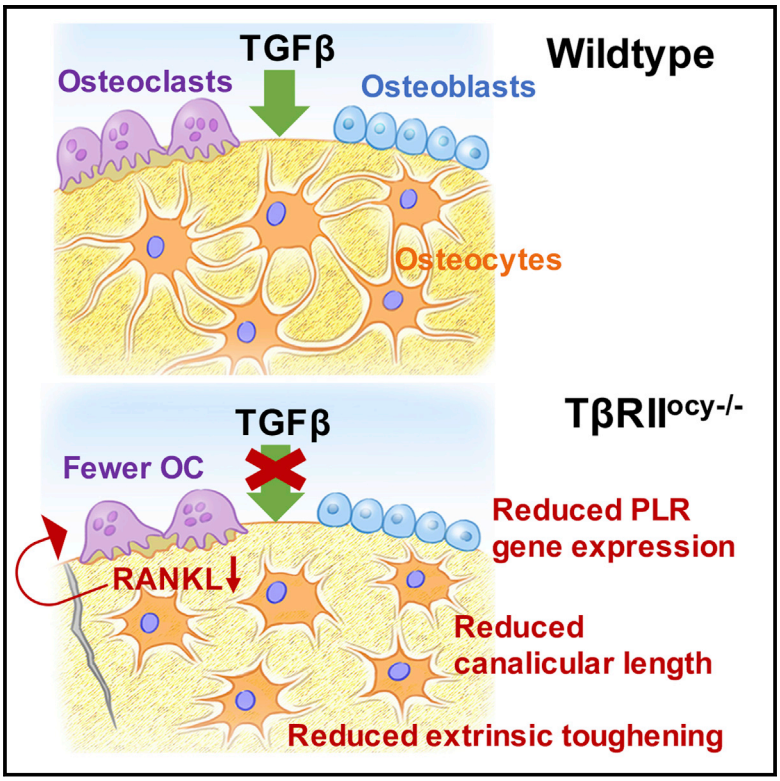

Highlights

- TGF-β is an osteocyte-intrinsic regulator of perilacunar/canalicular remodeling (PLR)
- Osteocytes actively maintain bone quality through regulated control of PLR
- Osteocytic PLR is the cellular mechanism by which TGF-β controls bone quality
- Defects in PLR cause severe bone fragility, even when bone mass is normal

Authors

Neha S. Dole, Courtney M. Mazur, Claire Acevedo, ..., Robert O. Ritchie, Khalid S. Mohammad, Tamara Alliston

Correspondence

tamara.alliston@ucsf.edu

In Brief

Resistance to fracture requires healthy bone mass and quality. However, the cellular mechanisms regulating bone quality are unclear. Dole et al. show that osteocyte-intrinsic TGF-β signaling maintains bone quality through perilacunar/canalicular remodeling. Thus, osteocytes mediate perilacunar/canalicular remodeling and osteoclast-directed remodeling to cooperatively maintain bone quality and mass and prevent fragility.

Dole et al., 2017, Cell Reports *21*, 2585–2596
November 28, 2017
https://doi.org/10.1016/j.celrep.2017.10.115

Cell Reports
Article

Osteocyte-Intrinsic TGF-β Signaling Regulates Bone Quality through Perilacunar/Canalicular Remodeling

Neha S. Dole,[1] Courtney M. Mazur,[1,2] Claire Acevedo,[1,3] Justin P. Lopez,[1,2] David A. Monteiro,[1,2] Tristan W. Fowler,[1] Bernd Gludovatz,[3] Flynn Walsh,[3] Jenna N. Regan,[4] Sara Messina,[3,5] Daniel S. Evans,[6] Thomas F. Lang,[7] Bin Zhang,[8] Robert O. Ritchie,[3,5] Khalid S. Mohammad,[4] and Tamara Alliston[1,2,9,*]

[1]Department of Orthopaedic Surgery, University of California, San Francisco, San Francisco, CA 94143, USA
[2]UC Berkeley/UCSF Graduate Program in Bioengineering, San Francisco, CA 94143, USA
[3]Materials Science Division, Lawrence Berkeley National Laboratory, Berkeley, CA 94720, USA
[4]Department of Medicine, Indiana University School of Medicine, Indianapolis, IN 46202, USA
[5]Department of Materials Science and Engineering, University of California, Berkeley, Berkeley, CA 94720, USA
[6]California Pacific Medical Center Research Institute, San Francisco, CA 94107, USA
[7]Department of Radiology and Biomedical Imaging, University of California, San Francisco, San Francisco, CA 94143, USA
[8]Department of Genetics & Genomic Sciences, Icahn Institute of Genomics and Multiscale Biology, Icahn School of Medicine at Mount Sinai, New York, NY 10029, USA
[9]Lead Contact
*Correspondence: tamara.alliston@ucsf.edu
https://doi.org/10.1016/j.celrep.2017.10.115

SUMMARY

Poor bone quality contributes to bone fragility in diabetes, aging, and osteogenesis imperfecta. However, the mechanisms controlling bone quality are not well understood, contributing to the current lack of strategies to diagnose or treat bone quality deficits. Transforming growth factor beta (TGF-β) signaling is a crucial mechanism known to regulate the material quality of bone, but its cellular target in this regulation is unknown. Studies showing that osteocytes directly remodel their perilacunar/canalicular matrix led us to hypothesize that TGF-β controls bone quality through perilacunar/canalicular remodeling (PLR). Using inhibitors and mice with an osteocyte-intrinsic defect in TGF-β signaling ($T\beta RII^{ocy-/-}$), we show that TGF-β regulates PLR in a cell-intrinsic manner to control bone quality. Altogether, this study emphasizes that osteocytes are key in executing the biological control of bone quality through PLR, thereby highlighting the fundamental role of osteocyte-mediated PLR in bone homeostasis and fragility.

INTRODUCTION

Bone fragility is determined by bone mass and quality. Bone quality encompasses parameters including bone geometry, porosity, trabecular microarchitecture, and bone extracellular matrix (ECM) material properties (Hernandez and Keaveny, 2006; Seeman, 2008). Historically, the prognosis of fragility fractures has focused on bone mass, but it is now known that compromised ECM properties play a causal role in bone fragility in diabetes, aging, and osteogenesis imperfecta (OI) (Delmas and Seeman, 2004; Fleischli et al., 2006; Grafe et al., 2014; Lane et al., 2006; Nalla et al., 2004; Ott, 1993; Van Staa et al., 2003). Despite the clinical importance of this and other aspects of bone quality, the management of fragility currently focuses on improving bone mass. Overcoming this clinical gap in diagnosing and treating bone quality requires elucidation of mechanisms that orchestrate the biological control of bone quality in skeletal health and disease.

Currently, the transforming growth factor beta (TGF-β) pathway is one of the few signaling pathways known to regulate bone mass and quality (Alliston, 2014; Balooch et al., 2005; Mohammad et al., 2009; Chang et al., 2010; Edwards et al., 2010). In bone, TGF-β produced by bone-forming osteoblasts is sequestered in the ECM in an inactive, latent form (Sinha et al., 1998). When released upon osteoclastic resorption of the ECM, TGF-β exerts pleiotropic effects on osteoblasts, osteoclasts, and their progenitors to coordinate bone remodeling (Dallas et al., 2008; Tang and Alliston, 2013). Aberration in TGF-β signaling leads to altered bone mass and poor bone quality in multiple skeletal diseases, including Camurati Engelman disease (CED) and OI (Grafe et al., 2014; Kinoshita et al., 2000). While the pathogenesis of the poor bone quality associated with these diseases has been attributed to imbalanced osteoclast and osteoblast activity, not much is known about the causal role of osteocytes and osteocyte-intrinsic TGF-β signaling in bone fragility.

In addition to regulating the activity of osteoclasts and osteoblasts, osteocytes also engage in perilacunar/canalicular remodeling (PLR), during which they directly resorb and deposit bone matrix surrounding their intricate lacuno-canalicular network (Qing and Bonewald, 2009). This process was originally called osteocyte osteolysis when it was observed in pathologic conditions or PLR in metabolically demanding situations such as lactation or hibernation (Haller and Zimny, 1977; Qing et al., 2012; Qing and Bonewald, 2009; Teti and Zallone, 2009; Wysolmerski, 2013). It is now clear that PLR is a homeostatic mechanism that helps to maintain mineral homeostasis and the lacuno-canalicular network. Several studies demonstrate the essential role in PLR of matrix metalloproteinases (Mmps; namely Mmp2, Mmp13, and Mmp14), cathepsin

K (Ctsk), carbonic anhydrase 2, and tartrate-resistant acid phosphatase (Acp5/TRAP) (Kogawa et al., 2013; Qing et al., 2012; Qing and Bonewald, 2009; Wysolmerski, 2013). Through loss-of-function studies in mice, these genes were found to be essential for an intact lacuno-canalicular network, organization of collagen, and bone matrix mineralization (Holmbeck et al., 2005; Inoue et al., 2006; Kogawa et al., 2013; Kulkarni et al., 2012; Qing and Bonewald, 2009; Tang et al., 2012; Tang and Alliston, 2013; Wysolmerski, 2013), all of which contribute to bone quality. Macro-mechanical testing of MMP13-deficient bones revealed a correlation between the loss of PLR and bone fragility (Tang et al., 2012). Nonetheless, many questions remain about the relationship between osteocyte-mediated PLR and bone quality.

In an effort to elucidate the cellular and molecular mechanisms that control bone quality, we tested the hypothesis that TGF-β acts directly on osteocytes to control PLR and that this mechanism accounts for the TGF-β-dependent control of bone quality. Several lines of evidence support this model, including the ability of TGF-β to directly regulate the expression of several Mmps implicated in PLR (Krstic and Santibanez, 2014; Selvamurugan et al., 2004). To investigate this possible mechanism, we employed unique *in vivo* and *in vitro* models and pharmacologic TGF-β antagonists similar to those in human clinical trials for the treatment of bone fragility in OI. Using this approach, we uncovered the essential role of osteocyte-intrinsic TGF-β signaling in the control of PLR and fracture resistance and demonstrate the importance of PLR in bone fragility.

RESULTS

Pharmacologic Inhibition of TGF-β Signaling Dysregulates PLR

We previously showed that pharmacologic inhibition of the TGF-β-receptor I (TβRI) kinase using SD-208 increases trabecular bone mass through stimulating osteoblastic bone formation and repressing osteoclastic resorption (Mohammad et al., 2009). However, the effect of SD-208 or other TβRI-inhibitory agents on osteocytes (OCYs) is unknown. To investigate the role of TGF-β signaling in osteocytes, the most abundant bone cells in cortical bone (Franz-Odendaal et al., 2006), we examined histologic and molecular outcomes of osteocyte-mediated PLR in mice treated with SD-208. As expected, 6 weeks of TβRI-inhibitor treatment significantly increased trabecular bone mass (Figure S1). Histologic analysis shows a dense and organized network of osteocyte canaliculi in cortical bone of vehicle-treated mice. However, TβRI-inhibitor treatment caused severe deterioration of the osteocyte canalicular network with a 50% reduction in canalicular length (Figures 1A and 1B).

The dysregulated canalicular network in TβRI kinase-inhibitor (TβRI-I)-treated bone resembles that seen in bones deficient in enzymes essential for PLR (Holmbeck et al., 2005; Inoue et al., 2006; Kulkarni et al., 2012; Tang et al., 2012). Therefore, we evaluated the effect of TβRI inhibition on the expression of genes encoding PLR enzymes, including *Mmp2*, *Mmp13*, and *Mmp14*, *Ctsk*, and *Acp5* in cortical bone. TβRI-I treatment coordinately reduced the level of mRNA encoding all five enzymes, relative to vehicle-treated controls (Figure 1C). Expression of the ATPase *Atp6v0d*, is increased in TβRI-I treated bone (Figure S2). Moreover, TβRI-I treatment also causes a decline in osteocytic protein expression of MMP13, MMP14, and CTSK without impacting their viability (Figures 1D–1F). This strong, concerted repression of several genes required for osteocyte-mediated PLR upon TGF-β inhibition indicates the critical role of TGF-β in controlling osteocyte function.

TGF-β Regulates PLR in a Cell-Intrinsic Manner

While systemic inhibitors of TGFβ clearly impact lacuno-canalicular networks and the expression of genes associated with PLR, it was unclear whether TGF-β exerts its effects on osteocytes directly or indirectly. Therefore, we examined the cell-intrinsic effects of TGF-β on MLO-Y4 osteocyte-like cells and OCY454 osteocytes, which more faithfully mimic osteocytic gene expression. Within 6 hr of treatment, TGF-β induced expression of *Mmp13*, *Mmp14*, and *Ctsk* mRNA, as well as *Serpine1*, a well-known TGF-β-inducible gene in MLO-Y4 cells (Figures 2A and 2B) (Graycar et al., 1989). TGF-β also induced expression of *Mmp13* and *Ctsk*, but not *Mmp14*, in OCY454 cells (Figures 2C and 2D). Further supporting the osteocyte-intrinsic role of TGF-β, TGF-β induced the expression of the osteocyte marker genes Sclerostin (*Sost*) and dentin matrix protein-1 (*Dmp1*) without affecting phosphate regulating endopeptidase homolog, X linked (*Phex*) (Figure S3).

In addition to expressing PLR enzymes, osteocytes engaged in PLR acidify their microenvironment. Using the pH-sensitive dye 5-(and-6)-carboxy SNARF-1, AM, we examined the effect of TGF-β on MLO-Y4 cell acidification. As shown by others (Kogawa et al., 2013), recombinant human sclerostin (rhSCL) induces PLR and lowers the intracellular pH (pHi) of MLO-Y4 cells. TGF-β treatment resulted in a larger acidification than sclerostin treatment. In contrast, blocking TGF-β signaling with an *in vitro* inhibitor of TβRI (SB-431542) relieved this acidification, such that pHi was equivalent to untreated cells (Figures 2E and 2F). Altogether, our findings support the possibility that TGF-β induces PLR in an osteocyte-intrinsic manner.

Osteocyte-Specific Inhibition of TGF-β Signaling Impairs PLR

To evaluate the osteocyte-intrinsic role of TGFβ signaling *in vivo*, TGF-β receptor II (TβRII) was deleted in osteocytes using DMP1-Cre mice, resulting in $T\beta RII^{ocy-/-}$ mice. We validated the specific reduction of TβRII expression in osteocytes (but not in other cell types) of $T\beta RII^{ocy-/-}$ bone relative to $DMP1^{Cre-/-}$; $T\beta RII^{fl/fl}$ (wild-type [WT]) littermate controls (Figures 3A and 3B). Abrogation of TGF-β signaling in $T\beta RII^{ocy-/-}$ bone was validated by reduced *TβRII* and *Serpine1* gene expression (Figure 3C). Furthermore, using primary bone marrow cultures from WT and $T\beta RII^{ocy-/-}$ mice, we verified the osteocyte-specific defect in TGF-β signaling by confirming that osteogenic gene expression is normal until after these cells differentiate into osteocytes (Figures S5A–S5D).

Because the systemic inhibition of TGF-β signaling causes severe deterioration of the osteocyte canalicular network, and because TGF-β regulates osteocytic expression of PLR enzymes, we evaluated the lacuno-canalicular network in

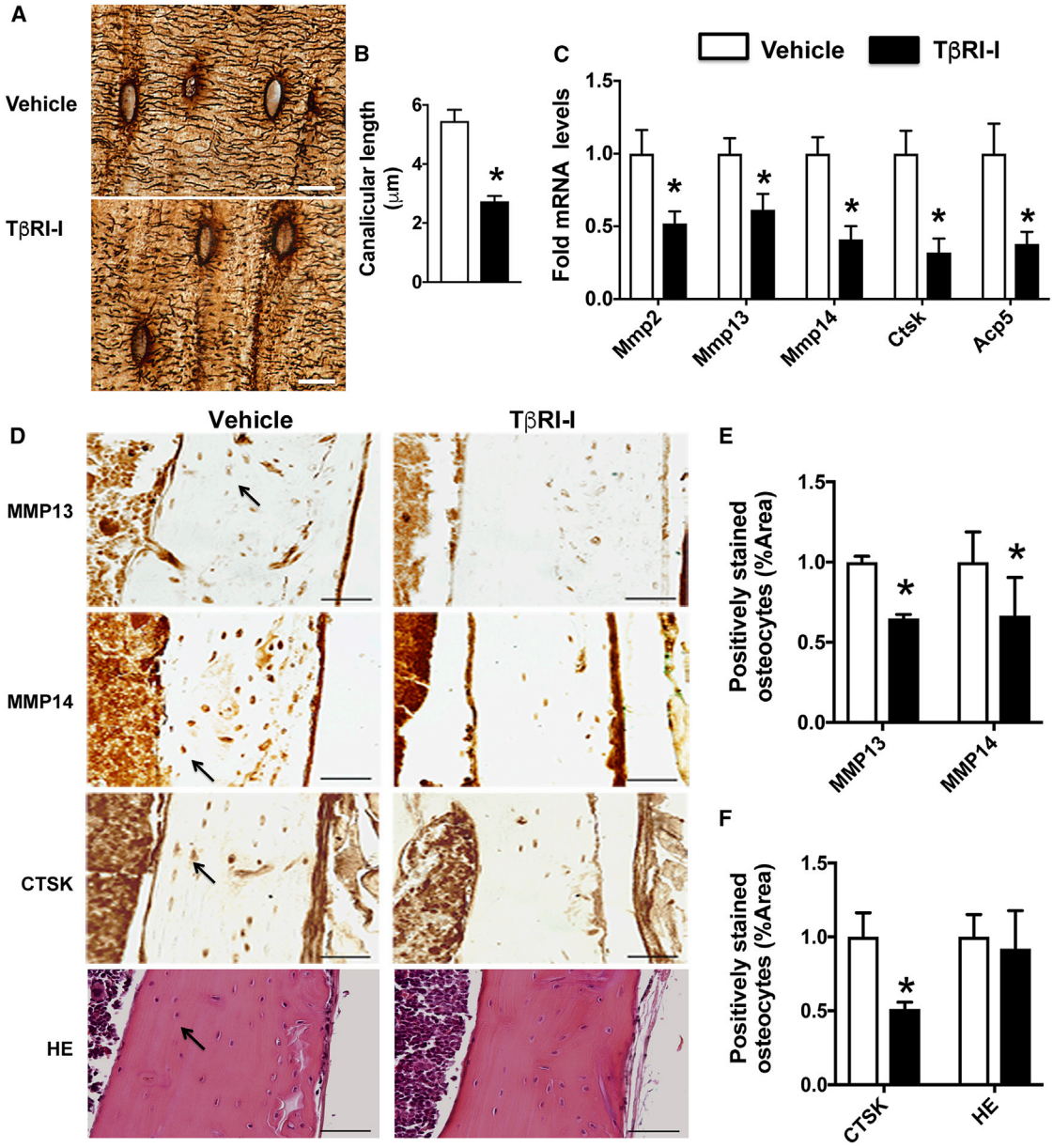

Figure 1. Pharmacologic TβRI Inhibition Impairs Perilacunar/Canalicular Remodeling

(A and B) Silver-nitrate-stained images of femoral cortical bone from mice treated with vehicle or TGF-β receptor I kinase inhibitor (TβRI-I; SD-208) treated mice show osteocyte lacuno-canalicular network (A) and canalicular length (B). Scale bar, 20 μm (n = 6 mice/group).

(C) qPCR analysis of the PLR genes *Mmp2*, *Mmp13*, *Mmp14*, *Ctsk*, and *Acp5* in bones from vehicle- and TβRI-I-treated animals (n = 8 mice/group).

(D–F) Immunohistochemistry (IHC) of MMP13, MMP14, and CTSK and H&E staining of femoral cortical bone of vehicle- and TβRI-I-treated animals. Arrows in the image indicate positively stained osteocytes (D). Osteocytes positive for MMP13 (E), MMP14 (E), CTSK (F), and HE (F) staining were quantified and normalized to total bone area. Scale bar, 50 μm (n = 4 mice/group).

Error bars indicate mean ± SEM; *p < 0.05 compared to vehicle from Student's t test.

TβRII$^{ocy-/-}$ cortical bone. Upon osteocytic deletion of TβRII, the canalicular network was abrogated and visibly blunted. Relative to WT, the length of canalicular projections in TβRII$^{ocy-/-}$ bone was reduced by 50% and the total lacuno-canalicular area was reduced by 32% (Figures 3D, 3E, and S4A).

Among the panel of PLR genes, expression of *Mmp2*, *Mmp13*, *Mmp14*, *Ctsk*, and *Acp5* was downregulated in TβRII$^{ocy-/-}$ mice (Figures 3F and S4B). In fact, the effect of osteocyte-intrinsic TβRII ablation on PLR gene expression was even more profound than that produced by TβRI-inhibitor treatment. Expression of osteocalcin (*Oc*), bone sialoprotein (*Ibsp*), *Dmp1*, and *Phex*, genes that control systemic mineral homeostasis, was unaffected by the absence of osteocytic TGF-β signaling. Expression of Sost, which is known to be induced by TGF-β

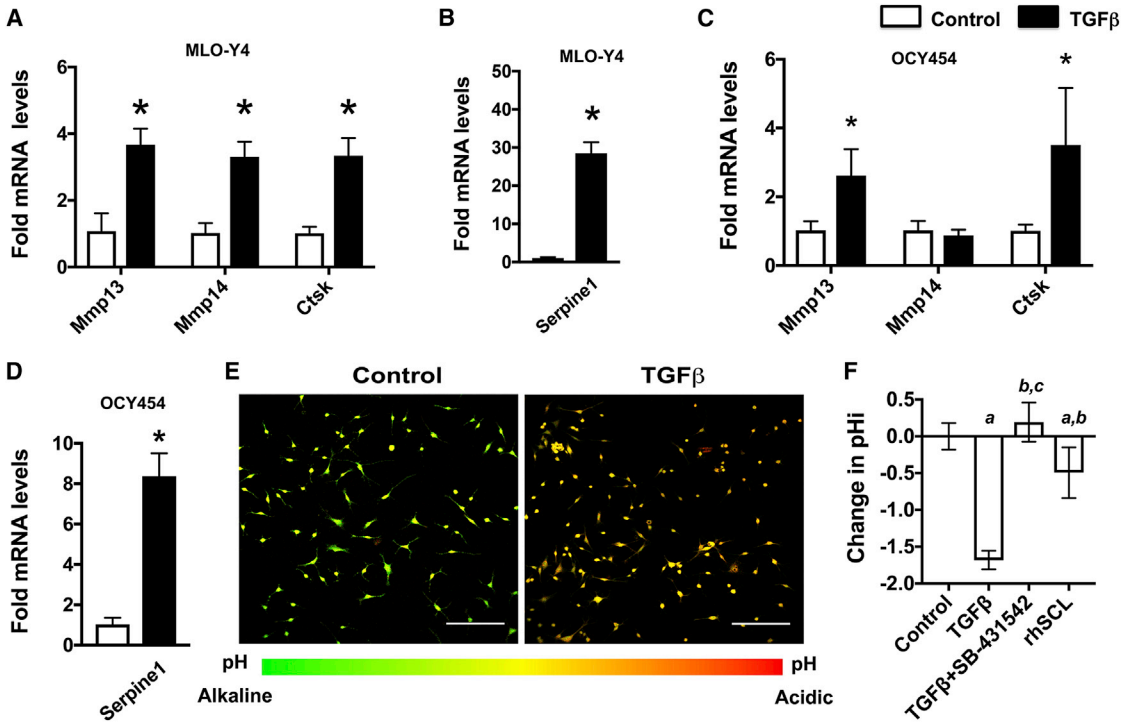

Figure 2. TGF-β Promotes Cell-Intrinsic Osteocytic Perilacunar/Canalicular Remodeling

(A and B) qPCR analysis of the PLR genes *Mmp13*, *Mmp14*, *Ctsk* (A), and *Serpine1* (B) upon TGF-β (5ng/mL) treatment in MLO-Y4 cells (n = 3 replicates/group). (C and D) qPCR analysis of the PLR genes *Mmp13, Mmp14, Ctsk* (C), and *Serpine1*(D) upon TGF-β (5ng/mL) treatment in OCY454 cells (n = 3 replicates/group). (E and F) Intracellular pH (pHi) of MLO-Y4 cells after 3 days of TGF-β (5 ng/mL), TβRI inhibitor SB-431542 (10 μM), or recombinant human sclerostin (rhSCL; 10 ng/mL) treatment. Representative image shows the shift in the emission peak from 580 nm to 640 nm after TGF-β treatment of MLO-Y4 cells (E). Scale bar, 100 μm. TGF-β-induced acidification is blocked by SB-431542 (F) (n = 4 replicates/group).

Error bars indicate mean ± SD of 3 independent experiments. *$p < 0.05$ different from control mRNA; $^{a}p < 0.05$ different from control pHi; $^{b}p < 0.05$ different from TGFβ pHi; $^{c}p < 0.05$ different from rhSCL pHi. Statistical significance was calculated using a Student's t test.

(Loots et al., 2012; Nguyen et al., 2013), was downregulated in TβRII$^{ocy-/-}$ bones (Figure 3G). Protein expression of MMP13, MMP14, and CTSK in osteocytes of TβRII$^{ocy-/-}$ mice was also significantly reduced 27%–40% compared to WT mice, without apparent changes in osteocyte number and viability as determined by H&E and TUNEL staining (Figures 3H, 3I, S4B, and S4C). These findings corroborated the observations in the TβRI-I mouse model and revealed the direct role of osteocytic TGF-β signaling in the regulation of PLR.

To rigorously evaluate the effect of TβRII deletion on lacunar size, orientation and shape, we utilized synchrotron radiation micro-tomography (SRμT), which visualizes and quantifies the osteocyte lacunae in a 3D space. In spite of the dramatic differences in the canalicular network seen histologically, osteocyte lacunar volume, shape, and orientation relative to the long axis of the bone did not differ significantly between TβRII$^{ocy-/-}$ and WT cortical bone (Figures 3J–3M and S4E–S4H). Also using SRμT, we detected a 3% reduction ($p = 0.06$) in peak bone mineral concentration in diaphyseal cortical bone of TβRII$^{ocy-/-}$ mice compared to WT (Figures 3M and S4H). Therefore, osteocyte-intrinsic TGF-β signaling regulates the expression of enzymes required for PLR and is essential for the integrity of the canalicular network and bone matrix mineralization. This not only reveals a previously unidentified role of TGF-β in osteocytes but also adds TGF-β to the short list of factors shown to regulate PLR.

Osteocyte-Specific Deletion of TβRII Increases Trabecular Bone Mass by Inhibiting Bone Resorption

Because alterations in TGF-β signaling often impact bone mass (Balooch et al., 2005; Mohammad et al., 2009), we analyzed the impact of ablated osteocyte-specific TGF-β signaling on trabecular and cortical bone mass and geometry. Bones of TβRII$^{ocy-/-}$ mice showed no gross abnormalities relative to WT mice. Microcomputed tomography (μCT) analysis revealed a 35% increase in trabecular bone mass in 8-week-old TβRII$^{ocy-/-}$ mice relative to WT littermates. This gain in mass was attributed to the corresponding increase in trabecular number (26%) and complementary decrease in trabecular spacing (25%) (Figures 4A–4D; Table 1). However, osteocytic deletion of TβRII did not affect cortical bone thickness or geometry (Figures 4K–4M). Cortical bone mineralization (Figure 4N) of TβRII$^{ocy-/-}$ mice was reduced by 4.8%, consistent with the 3% decrease in peak bone mineral concentration detected by SRμT (Figure 3M). Therefore, osteocyte-intrinsic TGF-β regulates the mass and geometry of trabecular, but not cortical, bone.

To understand the cellular mechanism underlying the elevated trabecular bone phenotype of TβRII$^{ocy-/-}$ mice,

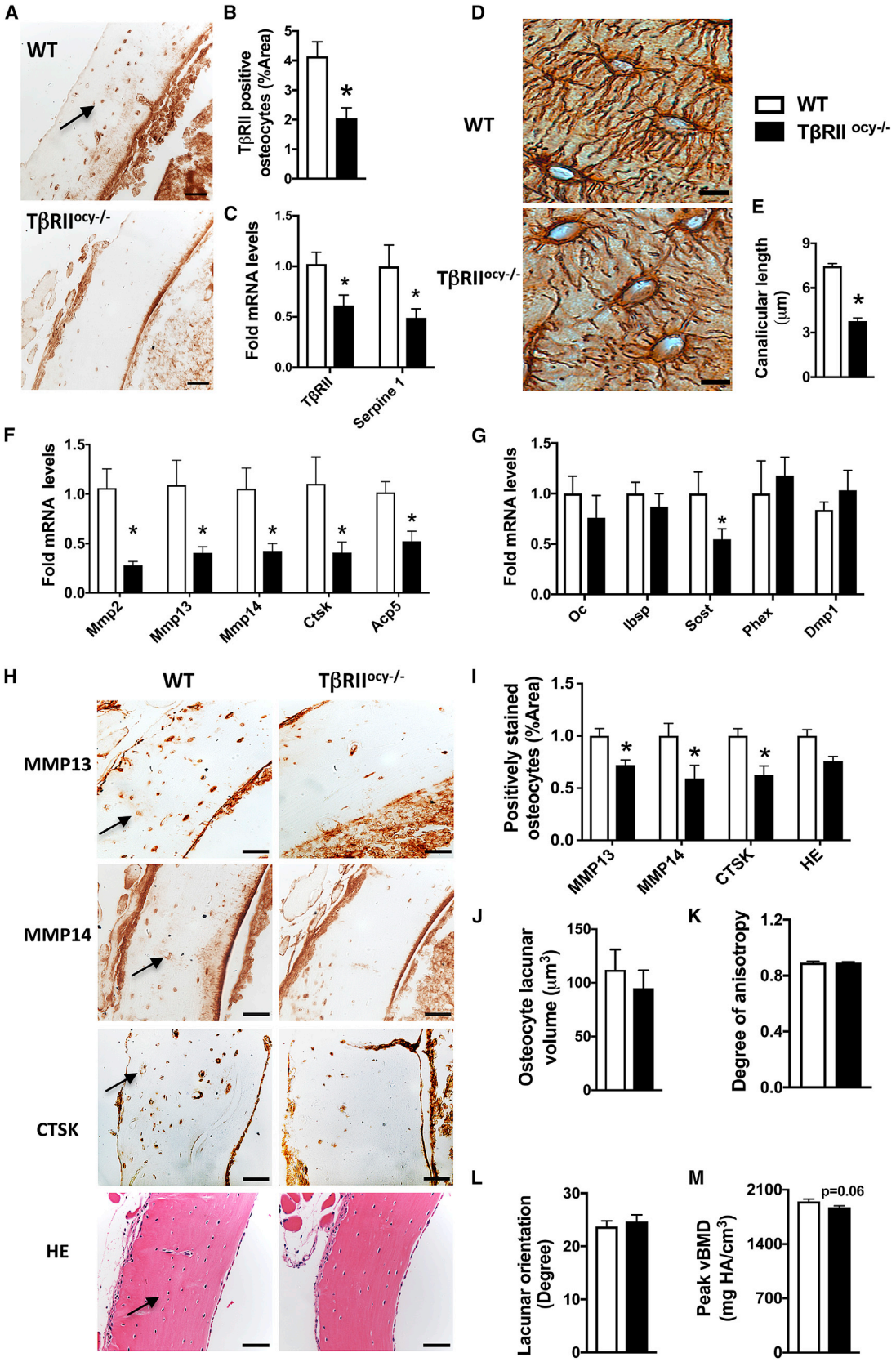

(legend on next page)

histomorphometry was performed. Neither static nor dynamic histomorphometric analyses revealed significant differences in osteoblast or bone formation parameters in TβRII$^{ocy-/-}$ bone (Figures 4E–4G; Table 1). On the other hand, measures of bone resorption implicate osteocyte-intrinsic TGF-β in the control of osteoclast function. Specifically, TRAP-positive osteoclasts were reduced by 40%, along with a 34% reduction in osteoclast surface in TβRII$^{ocy-/-}$ mice (Figures 4H and 4I; Table 1). Furthermore, TβRII$^{ocy-/-}$ mice showed a substantial reduction in the ratio of RANKL/OPG mRNA expression due to low levels of the osteoclastogenic factor RANKL (*Rankl*) but unaffected levels of OPG (*Opg*), a RANKL antagonist (Figures 4J, S5E, and S5F). Together, these results attribute the high trabecular bone mass phenotype of TβRII$^{ocy-/-}$ mice to decreased osteoclast function, which essentially results from decreased production of RANKL by TβRII-deficient osteocytes.

Osteocyte Deletion of TβRII Reduces Fracture Resistance of Bone

Given that TβRII$^{ocy-/-}$ cortical bone mass and thickness are normal, evidence of bone fragility in these mice would be consistent with defects in bone quality. Despite our prior implication of TGF-β in bone quality regulation (Balooch et al., 2005; Chang et al., 2010; Mohammad et al., 2009), the cellular target responsible for the control of bone quality has since been elusive. The disruption of PLR and cortical bone mineralization in TβRII$^{ocy-/-}$ bone led us to hypothesize that TGF-β controls bone quality through regulation of osteocytic PLR. To test this hypothesis, we performed a series of tests to evaluate the macromechanical and material behavior of TβRII$^{ocy-/-}$ bone.

Macromechanical testing showed reduced fracture resistance of TβRII$^{ocy-/-}$ cortical bone. Using flexural testing, we found that TβRII$^{ocy-/-}$ femora exhibited a 26% decline in the bending modulus relative to WT bone, indicating a reduced capacity to resist elastic deformation (Figure 5A). Similarly, the yield stress was reduced by 27% in TβRII$^{ocy-/-}$ bones (Figure 5B). Using nanoindentation to examine the material properties of the TβRII$^{ocy-/-}$ bone, we found that the Young's modulus was significantly lower in TβRII$^{ocy-/-}$ bone matrix than in WT bone matrix (Figure 5C), a finding that is consistent with the reduced TβRII$^{ocy-/-}$ cortical bone mineralization (Figure 4N). The most dramatic effects were observed in fracture toughness testing, in which notched TβRII$^{ocy-/-}$ cortical bone exhibited a 65% decrease in total work of fracture compared to WT bone (Figure 5D). These findings are particularly remarkable given that the severe fragility of TβRII$^{ocy-/-}$ bone could not be attributed to differences in cortical bone mass or geometry.

Accordingly, we sought to learn more about the material mechanisms responsible for TβRII$^{ocy-/-}$ bone fragility. For example, resistance to crack *initiation* is primarily imparted through intrinsic toughening mechanisms, representing a material's inherent resistance to microstructural damage. On the other hand, crack *growth* toughness stems from extrinsic toughening mechanisms, which act to shield the crack from the applied driving force to limit crack propagation (Launey and Ritchie, 2009).

To distinguish between the effects of osteocyte TβRII deficiency on crack initiation and crack growth, we conducted fracture toughness testing in a variable pressure scanning electron microscope to simultaneously visualize and quantify crack behavior. While crack initiation toughness could not be conclusively differentiated between genotypes, the shallow slope of the R-curve for TβRII$^{ocy-/-}$ bones is indicative of reduced crack growth toughness and a loss of extrinsic toughening mechanisms (Figure 5E). *In situ* images of crack growth show evidence of extrinsic toughening by crack deflection and uncracked ligament bridging in WT bone (Figure 5E, i–iii). Conversely, the path of cracks in TβRII$^{ocy-/-}$ bone tended to be more linear and shorter relative to their profile extension in WT bones (Figures 5F and 5G). Therefore, we conclude that TGF-β regulates bone quality in an osteocyte-intrinsic manner, specifically through extrinsic toughening mechanisms that limit crack growth. Identification of osteocytes as crucial cellular targets in the biological control of bone quality raises new questions about the role of osteocytes and PLR in human bone fragility.

DISCUSSION

This study advances our understanding of bone homeostasis and fragility by revealing an osteocyte-intrinsic role for TGF-β signaling. Here, we implicate TGF-β as a crucial regulator of PLR and pinpoint osteocytes as the cell type principally responsible for the biological control of bone quality. Using either pharmacologic TGF-β receptor type I kinase inhibitors or a genetic model of osteocyte-specific TGF-β receptor ablation, we demonstrate that suppression of TGF-β signaling causes a severe deterioration of osteocyte canalicular network and dysregulates the expression of a host of PLR genes. Loss of osteocyte-intrinsic TGF-β signaling also reduces bone matrix

Figure 3. Osteocytic Deletion of TβRII Dysregulates Perilacunar/Canalicular Remodeling

(A and B) TβRII-stained osteocytes (A) (arrow, scale bar, 50 μm) in the femoral cortical bone from WT and TβRII$^{ocy-/-}$ mice (8-week-old males) were quantified as percentage of positively stained osteocytes normalized to total bone area (B) (n = 5 mice/group).

(C) qPCR analysis of TβRII and Serpine1 in WT and TβRII$^{ocy-/-}$ femoral bones. (n = 8–10 mice/ group).

(D and E) Silver-nitrate-stained images of WT and TβRII$^{ocy-/-}$ femoral cortical bone shows the osteocyte lacuno-canalicular network (D) and canalicular length (E) (scale bar, 20 μm; n = 5 mice/group).

(F and G) qPCR analysis of the PLR genes *Mmp2*, *Mmp13*, *Mmp14*, *Ctsk*, and *Acp5* (F) and the osteocyte-specific genes *Sost*, *Dmp1*, and *Phex* (G) in WT and TβRII$^{ocy-/-}$ bones (n = 8–10 mice/group).

(H and I) Immunohistochemistry (IHC) of MMP13, MMP14, and CTSK and H&E staining of WT and TβRII$^{ocy-/-}$ femoral cortical bone. Arrows in the image indicate positively stained osteocytes (H) that were quantified and normalized to total bone area (I) (n = 4 mice/group).

(J–M) SRμT shows volume (J), degree of anisotropy (K), orientation (L), and mineralization (M) of osteocyte lacunae of WT and TβRII$^{ocy-/-}$ bone (n = 3–4 mice/ group).

Error bars indicate mean ± SEM; *p < 0.05 compared to WT from Student's t test.

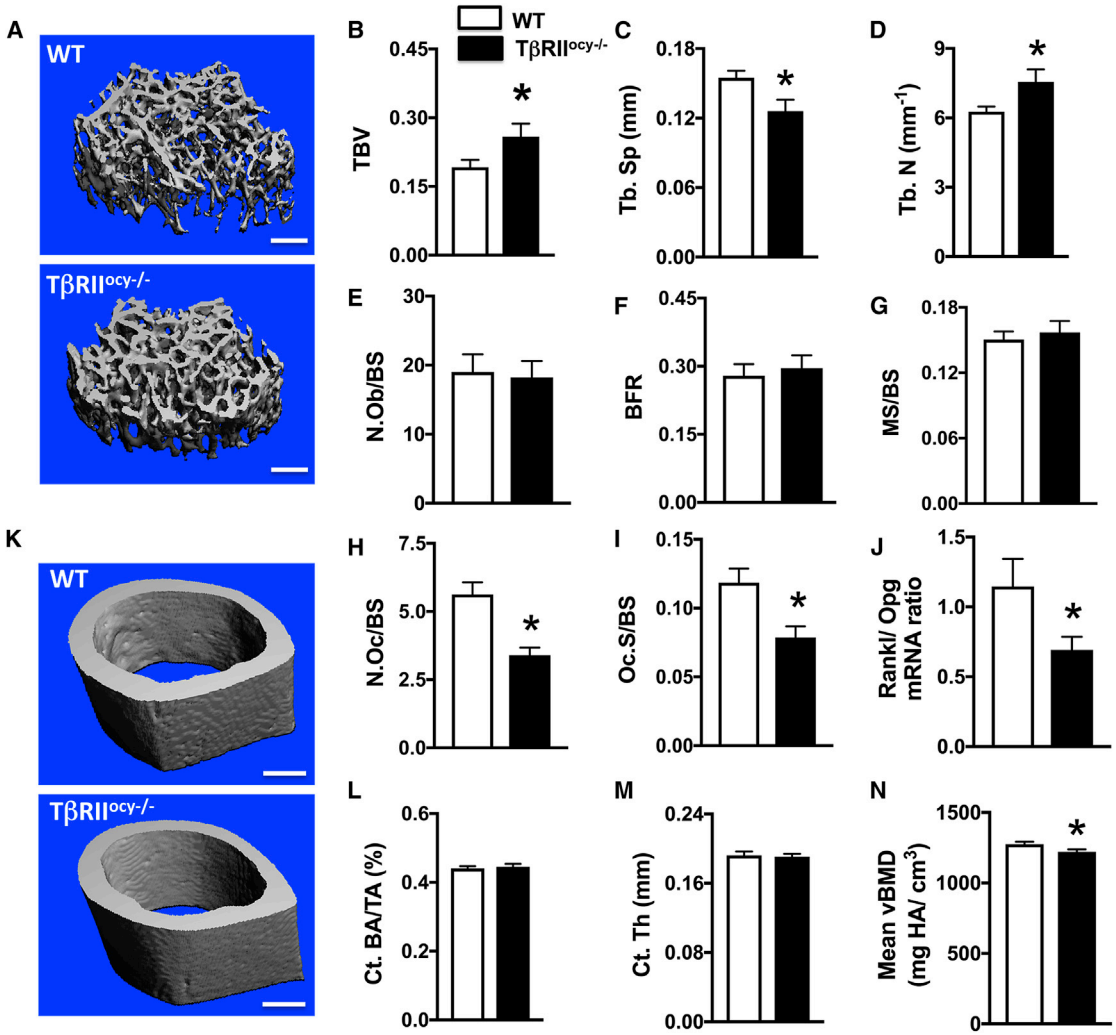

Figure 4. Osteocytic Deletion of TβRII Increases Trabecular Bone Mass but Does Not Affect Cortical Bone Mass

(A–D) μCT analysis of femur from WT and TβRII$^{ocy-/-}$ mice (8-week-old males). Representative μCT reconstructions of trabecular bone (A) from mice and trabecular bone parameters: trabecular bone volume fraction (BV/TV) (B), trabecular number (Tb.N.) (C), and separation (Tb.Sp.) (D). Scale bar, 100 μm (n = 10–11 mice/group).

(E–I) Histomorphometric analysis of femurs from WT and TβRII$^{ocy-/-}$ mice (8-week-old males) measures osteoblast number normalized to bone surface (N.Ob/BS) (E), bone formation rate (BFR) (F), percent mineralizing bone surface per bone surface (MS/BS) (G), osteoclast number normalized to bone surface (N.Oc/BS) (H), and osteoclast surface normalized to bone surface (Oc.S/BS) (I) (n = 6–7 mice/group).

(J) qPCR analysis of mRNA harvested from WT and TβRII$^{ocy-/-}$ bones shows the *Rankl*/*Opg* ratio (n = 8–10 mice/group).

(K–N) Representative μCT reconstructions of femoral cortical bone femur from WT and TβRII$^{ocy-/-}$ mice (8-week-old males) (K) and the cortical bone parameters cortical area fraction (Ct. BA/TA) (L), cortical thickness (Ct. Th) (M), and cortical mineralization (Ct. Min) (N). Scale bar, 100 μm (n = 10–11 mice/group).

Data are presented as mean ± SEM; *p < 0.05 compared to WT from Student's t test.

mineralization. Because TβRII$^{ocy-/-}$ cortical bone mass and geometry are normal, the profound fragility of these bones reveals that TGF-β controls bone quality through an osteocyte-intrinsic mechanism that relies on PLR. These findings strongly support the idea that PLR plays a fundamental role in bone homeostasis, specifically as the cellular mechanism responsible for the maintenance of the lacuno-canalicular network and bone quality.

Our findings revealed TGF-β signaling to be a cell-intrinsic regulator of PLR. Osteocyte-specific inhibition of TGF-β signaling decreases the expression of several genes that have been functionally implicated in PLR, including *Mmp2*, *Mmp13*, *Mmp14*, *Ctsk*, and *Acp5*. The coordinated regulation of these PLR genes by TGF-β is consistent with the effects of other PLR-regulatory pathways. Most of these genes are induced by PLR agonists, such as sclerostin and PTH, but repressed by PLR antagonists, such as glucocorticoids (Fowler et al., 2017; Kogawa et al., 2013; Qing et al., 2012). In each case, including in this study, these changes in gene expression correspond to alterations in the organization of the canalicular network. Interestingly, expression of vacuolar ATPases that function in osteocyte acidification are upregulated in TβRII$^{ocy-/-}$ bone, raising the possibility that a feedback loop compensates for the low level of proteases mediating PLR.

Table 1. Skeletal Phenotyping of 8-Week-Old WT and TβRII$^{ocy-/-}$ Mice

Parameters	WT	TβRII$^{ocy-/-}$
μCT		
Distal Femur		
TBV (BV/TV) (%)	0.192 ± 0.016	0.259 ± 0.028[a]
Conn D (1/mm^3)	377.74 ± 29.29	493.37 ± 71.58
Tb. N (1/mm)	6.275 ± 0.215	7.557 ± 0.542[a]
Tb. Th (μm)	0.043 ± 0.002	0.043 ± 0.001
Tb. Sp (mm)	0.155 ± 0.006	0.126 ± 0.009[a]
SMI	1.720 ± 0.184	1.063 ± 0.287[b]
Tb. Min (mg HA/cm^3)	1,020.98 ± 9.31	1,014.23 ± 13.36
Midshaft Femur		
Ct. BA/TA (%)	0.437 ± 0.006	0.445 ± 0.008
Ct. Th (μm)	0.188 ± 0.004	0.189 ± 0.003
Ct. SMI	−0.442 ± 0.239	−1.066 ± 0.339
Ct. Min (mg HA/cm^3)	1,279.69 ± 15.30	1,217.59 ± 16.136[a]
Histomorphometry		
Static parameters		
OV/BV	0.007 ± 0.001	0.004 ± 0.001
OS	0.14 ± 0.02	0.12 ± 0.04
OS/BS (%)	0.04 ± 0.01	0.03 ± 0.01
O. Wi (μm)	3.28 ± 0.21	2.79 ± 0.36
N.Ob	61.00 ± 5.61	60.94 ± 8.81
N.Ob/BS (/mm)	19.01 ± 2.57	18.24 ± 2.38
Oc.S	0.83 ± 0.07	0.68 ± 0.01[c]
Oc.S/BS (%)	0.12 ± 0.01	0.08 ± 0.01[a]
N.Oc	39.57 ± 3.10	30.17 ± 1.66[a]
N.Oc/BS (/mm)	5.63 ± 0.44	3.40 ± 0.28[a]
Dynamic Parameters		
MS/BS (%)	0.15 ± 0.01	0.16 ± 0.01
MAR (μm/d)	1.84 ± 0.13	1.89 ± 0.17
BFR/BS (μm^2. μm^3. d)	0.28 ± 0.03	0.30 ± 0.03

μCT and histomorphometry analysis revealed significant differences in trabecular bone phenotype, cortical mineralization, and osteoclast behavior between wild-type and TβRII$^{ocy-/-}$ mice, but no differences were observed in cortical bone volume or osteoblast behavior. Bone parameters measured by μCT include trabecular bone volume fraction (TBV), connectivity density (Conn D), trabecular number (Tb. N), trabecular thickness (Tb. Th), trabecular separation (Tb. Sp), structural model index (SMI), trabecular mineralization (Tb. Min), cortical bone volume fraction (Ct. BV/TV), cortical thickness (Ct. Th), cortical SMI, and cortical mineralization (Ct. Min), with n = 10–11 mice per group. Histomorphometry parameters measured include osteoid volume (OV/BV), osteoid surface (OS), osteoid width (O. Wi), osteoblast number (N. Ob), osteoblast surface (N. Ob/BS), osteoclast surface (Oc.S), eroded bone surface (Oc.S/BS), osteoclast number (N. Oc), osteoclast number (N.Oc/BS), mineralization surface (MS/BS), bone formation rate (BFR), and mineral apposition rate (MAR), with n = 6–7 mice per group. Data are presented as mean ± SEM.

[a]$p < 0.05$ versus WT group, Student's t test.
[b]$p = 0.06$ versus WT group, Student's t test.
[c]$p = 0.07$ versus WT group, Student's t test.

The effects of TGF-β and other PLR-regulatory pathways on the lacuno-canalicular network and on bone matrix differ in important ways. In addition to alterations in the canalicular network, lactation and glucocorticoid treatment cause changes in lacunar size (Fowler et al., 2017; Qing et al., 2012). Furthermore, collagen organization is disrupted in MMP13-deficient mice and in mice treated with glucocorticoids. In TβRII$^{ocy-/-}$ mice, neither collagen organization nor lacunar volume, shape, and orientation were impacted. In this study, PLR-mediated changes were observed at osteocyte canaliculi alone. Interestingly, emerging data from our lab and others (Fowler et al., 2017; Kaya et al., 2017; Tang et al., 2012) suggest that remodeling by osteocytes may be spatially defined, such that some circumstances favor remodeling at lacunae, whereas others will promote remodeling around canaliculi. Additional studies will be needed to determine the extent to which this is true.

The *in vitro* analysis of osteocyte acidification is a useful surrogate of PLR, but additional research is needed to better understand the cell biology of PLR. Nonetheless, TGF-β clearly acts directly on osteocytes to calibrate the extent of PLR and is required for the maintenance of the lacuno-canalicular network. Importantly, it is possible that the degenerated canalicular networks in our mouse models of impaired TGF-β signaling result from defective osteocyte integration into the bone matrix. A shorter time course or an inducible model would be needed to conclusively address this question. However, our previous studies have shown similar canalicular degeneration within 21 days of glucocorticoid treatment (Fowler et al., 2017) or a week of lactation (unpublished data) (Kaya et al., 2017; Qing et al., 2012; Qing and Bonewald, 2009; Wysolmerski, 2013), thereby indicating that changes in the canalicular network can occur rapidly in a manner that is independent of a maturation defect.

The critical role of TGF-β in osteocytes complements its actions in osteoblasts, osteoclasts, and their progenitors, where it couples bone formation to resorption (Dallas et al., 2008). Thus, it is not surprising that osteocyte-intrinsic ablation of TβRII would inhibit osteoclast function due to reduced levels of RANKL expression by osteocytes. Whether by systemic TβRI inhibition, expression of a dominant negative TGFβ type II receptor in osteoblasts, or in TβRII$^{ocy-/-}$ mice, trabecular bone mass is increased due to reduced RANKL expression and reduced osteoclastogenesis (Edwards et al., 2010; Filvaroff et al., 1999; Mohammad et al., 2009). Though we cannot completely exclude a causal role of TβRII$^{ocy-/-}$ osteocyte canalicular degeneration in the trabecular bone phenotype, our current and previous data suggest that TGF-β's regulation of RANKL expression is cell intrinsic. On the other hand, the complexity of TGF-β crosstalk in bone underlies the unique, and at times apparently contradictory, bone phenotypes that result from manipulating TGF-β signaling in one cell type or another (Dallas et al., 2008; Tang and Alliston, 2013). Furthermore, in bone and in many other tissues, the effect of TGF-β is nonlinear, such that either increased or decreased TGF-β signaling can produce an osteoporotic phenotype (Balooch et al., 2005; Borton et al., 2001; Erlebacher and Derynck, 1996). Despite this known complexity, we were surprised by the low mineral concentration of TβRII$^{ocy-/-}$ bone,

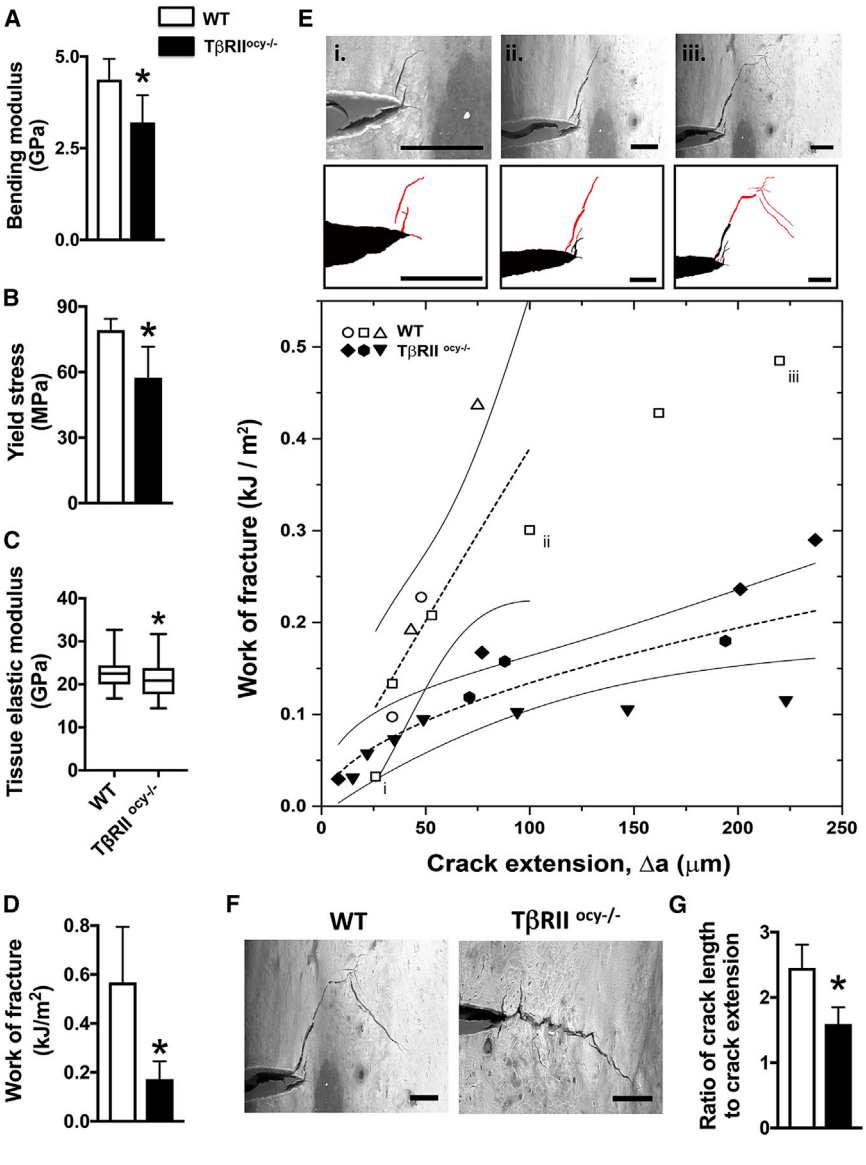

Figure 5. Osteocytic Deletion of TβRII Reduces Bone Material Properties at Multiple Length Scales

Mechanical testing on femurs from WT and TβRII$^{ocy-/-}$ (8-week-old males).

(A–B) Flexural tests of intact femurs shows bending modulus (A) and yield stress (B) (n = 5 mice/group).

(C) Nanoindentation of mid-diaphyseal femoral bone shows that tissue elastic modulus (n = 3 mice/group).

(D–E) *In situ* fracture toughness testing of notched femurs subjected to 3-point bending in a variable pressure SEM shows total work of fracture (WoF) (D) (n = 5 mice/group) and WoF R-curves produced by calculating WoF at each instance of crack propagation (E) (n = 3 mice/group). Three stages of crack growth are shown for a WT sample (i–iii) (scale bar, 100 μm), with pre-existing notch or crack in black and new crack extension in red, and the corresponding points are indicated in the R-curve.

(F–G) The decrease in TβRII$^{ocy-/-}$ bone of the extrinsic toughening mechanism, crack deflection, is readily seen in two representative samples (F) (scale bar, 100 μm) and in quantification of the ratio of total crack length to crack extension (G) (n = 5 mice/group).

Data are presented as mean SD. 95% confidence intervals in (E) are calculated based on a power fit. *p < 0.05 different from WT group from Student's t test.

given that mineralization is increased by systemic post-natal TβRI-I treatment (Edwards et al., 2010; Mohammad et al., 2009). Given that osteocyte canaliculi are sites of secondary mineralization, it is possible that the reduced canalicular length in the TβRII$^{ocy-/-}$ bones reduces surface area available for mineralization. Moreover, the increased expression of vacuolar ATPase may create an acidic microenvironment that is unfavorable for mineralization. Additional studies will be needed to discern the mechanisms by which pharmacologic disruption of TGF-β signaling affects bone mineralization differently from genetic ablation of TβRII specifically in osteocytes.

Bone strength relies on bone mass and bone quality, both of which depend on the ability of TGF-β to coordinate the function of osteoblasts, osteoclasts, and osteocytes. In spite of the fact that bone quality contributes to at least half of fractures in people with clinically normal bone mass (Schuit et al., 2004; Sornay-Rendu et al., 2007), the cellular mechanisms controlling bone quality have remained unclear. Understanding these mechanisms is a critical step in improving the diagnostics and therapeutics for fragility fractures (Hernandez and Keaveny, 2006; Seeman, 2008). This study represents the most definitive evidence so far implicating osteocyte-mediated PLR in the control of bone quality. Previous studies by our group and others show that bone quality is impaired following glucocorticoid treatment or systemic ablation of MMP13 and that PLR is impaired in each case (Fowler et al., 2017; Lane et al., 2006; Tang et al., 2012). Here, we find that osteocyte-specific deletion of TGF-β signaling caused defects in PLR, cortical bone mineralization, flexural strength, ECM material properties, and fracture toughness without impacting cortical bone mass. In diseases like Camurati Engelman syndrome and OI, both of which are characterized by excessive TGF-β signaling (Grafe et al., 2014; Kinoshita et al., 2000; Tang et al., 2009), deregulation of osteocyte-mediated remodeling may contribute to bone fragility. Similarly, the extent to which dysregulated PLR contributes to the fragility in other skeletal diseases, including renal osteodystrophy, secondary hyperparathyroidism, and glucocorticoid-induced osteoporosis, is an important area of further investigation. If so, PLR could be an attractive therapeutic target for improving fracture resistance in many conditions.

In conclusion, this study emphasizes the need to identify the cellular and molecular mechanisms regulating bone quality to develop new therapies to address the significant unmet clinical need for the treatment of bone fragility. Current therapeutics can improve 70% of trabecular fractures but only 20%–40% of cortical bone fractures, which is precisely where PLR dysregulation is most profound (Ahmed et al., 2015; Chen and Sambrook, 2011; Rivadeneira and Mäkitie, 2016). A combination of systems analysis of genome-wide association study (GWAS) data from clinical cohorts, along with functional *in vivo* and *in vitro* studies, can shed light on new molecular targets to control bone fragility and expand the pool of genetic markers needed for fracture risk assessment and prevention.

EXPERIMENTAL PROCEDURES

Mice

To block TGF-β signaling systemically, 5-week-old C57BL/6 male mice of equal weight were administered either vehicle (1% methylcellulose) or a specific inhibitor of TGFβRI (SD-208, 60 mg/kg twice daily by oral gavage) for 6 weeks (Mohammad et al., 2009). We also generated mice with osteocyte-specific ablation of TβRII), which effectively blocks osteocyte sensitivity to TGF-β ligand. Homozygous TβRII-floxed mice that possess *loxP* sites flanking exon 4 of the targeted gene were backcrossed for 3 generations into a C57BL/6 background and subsequently bred with hemizygous −10kb-DMP1-Cre$^{+/-}$ mice, which express Cre recombinase primarily in osteocytes (Levéen et al., 2002; Lu et al., 2007). Half of the mice from the resulting cross were DMP1-Cre$^{+/-}$;TβRII$^{fl/fl}$ (named TβRII$^{ocy-/-}$ mice) and half were DMP1-Cre$^{-/-}$;TβRII$^{fl/fl}$ littermate controls (WT mice), as confirmed by PCR genotyping. All animal procedures were approved by the Institutional Animal Care and Use Committee of the University of California, San Francisco and the Indiana University School of Medicine.

Morphological Analysis

For skeletal phenotyping, femurs harvested from 8-week-old male mice (n = 8 mice per group) were cleaned of soft tissue and fixed in 10% neutral buffered formalin for μCT. For μCT, fixed femurs were stored in 70% ethanol. For histomorphometry, 7-week-old male mice were administered with two intraperitoneal injections of calcein (20 mg/kg body weight, Sigma) 10 and 3 days prior to euthanasia. The harvested femurs were fixed in 10% neutral buffered formalin for 48 hr, processed, and embedded in a methylmethacrylate resin (MMA) plastic resin. Additional details of μCT and histomorphometry procedures are described in Supplemental Experimental Procedures.

qRT-PCR Analysis

We purified RNA from cells in culture and from bones dissected from soft tissues using the miRNeasy mini kit (QIAGEN, Valencia, CA) following the manufacturer's protocol. *In vitro* results are representative of n = 3 replicates per group and 3 independent experiments. For bones (humeri from n ≥ 8 mice per group), proximal and distal regions were cut off and marrow was removed by centrifugation before RNA extraction. The majority of RNA obtained from bone using this method is osteocyte derived, with very little contribution from osteoblasts (Halleux et al., 2012). Additional details of qRT-PCR analysis are described in Supplemental Experimental Procedures).

Immunohistochemistry

For immunohistochemistry, paraffin-embedded (7 μm thick) sections were incubated with primary antibodies for anti-MMP13 (1:100; Abcam, ab39012), anti-MMP14 (1:100; Abcam, ab38971), anti-CTSK (1:75; Abcam, ab19027), or anti-TβRII (1:500; Abcam, ab186838). This was followed by incubation with corresponding biotinylated secondary antibody, avidin-conjugated peroxidase, and diaminobenzidine substrate chromogen system (Innovex Universal Animal IHC kit). Corresponding nonimmune immunoblobulin Gs (IgGs) were used as negative controls. H&E and TUNEL-DAPI staining were performed to visualize osteocyte number and apoptosis. Ploton silver staining (Jáuregui et al., 2016; Ploton et al., 1986) was performed for visualization of the osteocyte lacuno-canalicular network. Images were acquired using a Nikon Eclipse E800 bright-field microscope and analyzed with ImageJ. Sections were evaluated for one femur from each of n ≥ 4 mice per group. Additional details of immunohistochemistry and image analysis are described in Supplemental Experimental Procedures.

Cell Culture

The MLO-Y4 osteocyte-like cell line (generously provided by L. Bonewald) was maintained in α-MEM supplemented with 2.5% fetal bovine serum, 2.5% bovine calf serum, and 1% penicillin-streptomycin. The OCY454 osteocyte cell line (generously provided by P. Divieti-Pajevic) was cultured in α-minimum essential media (α-MEM) supplemented with 10% fetal bovine serum and 1% antibiotic/ antimycotic (Gibco). For treatment, cells were cultured in α-MEM containing 0.5%–1% fetal bovine serum supplemented with 5 ng/mL TGF-β1 (Humanzyme, HZ-1011), 10 μM SB431542 (Sigma, S4317), or 10 ng/mL rhSCL (R&D Systems) for the indicated times.

pHi Assay

pHi was measured in transfected or untransfected MLO-Y4 cells treated with TGF-β1, SB431542, or rhSCL using the pH-sensitive fluorescent dye 5-(and-6)-carboxy SNARF-1, AM (Molecular Probes) as described previously (Kogawa et al., 2013). Briefly, after 3 days of culture in the indicated conditions, cells were washed with PBS and loaded with 5-(and-6)-carboxy-SNARF-1, AM at 37°C for 30 minutes, at a final concentration of 10 μM and visualized under a Leica TCS SPE confocal microscope (n = 4 replicates per group and 3 independent experiments). Additional details of the procedure are provided in Supplemental Experimental Procedures.

SRμT

SRμT studies were used to assess the degree of mineralization of bone as well as the volume and degree of anisotropy of osteocyte lacunae. The mid-diaphysis of 8-week-old male mouse femurs were scanned with 20 keV X-ray energy, with a 300 ms exposure time, using a 5× magnifying lens for a spatial resolution of 1.3 μm (n = 3–4 mice/ group). Additional details of the SRμT procedure are described in Supplemental Experimental Procedures.

Mechanical Tests

To measure bone quality, we assessed the macromechanical properties and the bone matrix material properties using flexural strength tests, *in situ* fracture toughness tests, and nanoindentation. Briefly, from 8-week-old TβRII$^{ocy-/-}$ and WT mice (n = 3–5 mice per group), intact femurs were isolated, cleaned of soft tissue, and stored in Hanks' balanced salt solution (HBSS). Details of the flexural strength tests, *in situ* fracture toughness tests, and nanoindentation procedures are described in Supplemental Experimental Procedures.

Statistical Analysis

All values are expressed as mean ± SEM or mean ± SD as appropriate for each assay. Group sizes were determined by power calculations providing 80% probability of detecting a significant difference ($p \leq 0.05$). Group size "n" is denoted in the figure legends. For *in vivo* data, n refers to the number of mice analyzed per group. For *in vitro* data, n refers to the number of independent experiments performed. An unpaired two-tailed Student's t test was used to compare the means of two groups using GraphPad Prism (GraphPad Software). Data points falling more than 2 SDs from the mean were excluded. Variances ranged from 12.5% to 20% and were similar between groups. No blinding was used during analysis. In all figures, $p \leq 0.05$ was considered statistically significant.

SUPPLEMENTAL INFORMATION

Supplemental Information includes Supplemental Experimental Procedures, five figures, and one table and can be found with this article online at https://doi.org/10.1016/j.celrep.2017.10.115.

AUTHOR CONTRIBUTIONS

Conceptualization, N.S.D, T.W.F., K.S.M., and T.A.; Investigation, N.S.D., C.M.M., C.A., J.P.L., D.A.M., B.G., J.N.R., F.W., D.S.E., T.F.L., and B.Z.; Data Curation, S.M.; Analysis, all authors; Writing – Original Draft, N.S.D.; Writing – Review & Editing, all authors; Visualization, N.S.D., C.M.M., and T.A.; Supervision, R.O.R., K.S.M., and T.A.; Project Leadership, N.S.D. and T.A.; Funding Acquisition, T.A.

ACKNOWLEDGMENTS

The authors gratefully acknowledge J.J. Woo for expert technical assistance. Illustration was kindly provided by Dr. M. Ouchida. This research was supported by NIH-NIDCR grant R01 DE019284 (T.A.), Department of Defense (DoD) grant PRORP OR130191 (T.A.), NSF grant 1636331, NIH-NIAMS grant R21 AR067439, NIH-NIAMS grant P30 AR066262-01 (T.A.), the Read Research Foundation (T.A.), OREF/ORS postdoctoral fellowship grant 17-008 (N.S.D.), NIH grant T32 GM008155 (C.M.M., J.P.L., and D.A.M.), NSF grant 1650113 (C.M.M.), a DoD National Defense Science & Engineering graduate (NDSEG) fellowship (D.A.M.), and Swiss National Science Foundation grant P300P2_167583 (C.A.).The authors acknowledge the use of the x-ray synchrotron beamlines 8.3.2 at the Advanced Light Source (ALS) at LBNL. The ALS is supported by the Director (Office of Science, Office of Basic Energy Sciences) of the U.S. Department of Energy under contract DE-AC02-05CH11231.

Received: June 13, 2017
Revised: September 26, 2017
Accepted: October 29, 2017
Published: November 28, 2017

REFERENCES

Ahmed, L.A., Shigdel, R., Joakimsen, R.M., Eldevik, O.P., Eriksen, E.F., Ghasem-Zadeh, A., Bala, Y., Zebaze, R., Seeman, E., and Bjørnerem, Å. (2015). Measurement of cortical porosity of the proximal femur improves identification of women with nonvertebral fragility fractures. Osteoporos. Int. *26*, 2137–2146.

Alliston, T. (2014). Biological regulation of bone quality. Curr. Osteoporos. Rep *12*, 366–375.

Balooch, G., Balooch, M., Nalla, R.K., Schilling, S., Filvaroff, E.H., Marshall, G.W., Marshall, S.J., Ritchie, R.O., Derynck, R., and Alliston, T. (2005). TGF-beta regulates the mechanical properties and composition of bone matrix. Proc. Natl. Acad. Sci. USA *102*, 18813–18818.

Borton, A.J., Frederick, J.P., Datto, M.B., Wang, X.F., and Weinstein, R.S. (2001). The loss of Smad3 results in a lower rate of bone formation and osteopenia through dysregulation of osteoblast differentiation and apoptosis. J. Bone Miner. Res. *16*, 1754–1764.

Chang, J.L., Brauer, D.S., Johnson, J., Chen, C.G., Akil, O., Balooch, G., Humphrey, M.B., Chin, E.N., Porter, A.E., Butcher, K., et al. (2010). Tissue-specific calibration of extracellular matrix material properties by transforming growth factor-β and Runx2 in bone is required for hearing. EMBO Rep. *11*, 765–771.

Chen, J.S., and Sambrook, P.N. (2011). Antiresorptive therapies for osteoporosis: a clinical overview. Nat. Rev. Endocrinol. *8*, 81–91.

Dallas, S.L., Alliston, T., and Bonewald, L.F. (2008). Transforming growth factor-beta. In Principles of Bone Biology, L.G.R.J.P. Bilezikian and G.A. Rodan, eds. (Academic Press), pp. 1145–1166.

Delmas, P.D., and Seeman, E. (2004). Changes in bone mineral density explain little of the reduction in vertebral or nonvertebral fracture risk with anti-resorptive therapy. Bone *34*, 599–604.

Edwards, J.R., Nyman, J.S., Lwin, S.T., Moore, M.M., Esparza, J., O'Quinn, E.C., Hart, A.J., Biswas, S., Patil, C.A., Lonning, S., et al. (2010). Inhibition of TGF-beta signaling by 1D11 antibody treatment increases bone mass and quality in vivo. J. Bone Miner. Res. *25*, 2419–2426.

Erlebacher, A., and Derynck, R. (1996). Increased expression of TGF-beta 2 in osteoblasts results in an osteoporosis-like phenotype. J. Cell Biol. *132*, 195–210.

Filvaroff, E., Erlebacher, A., Ye, J., Gitelman, S.E., Lotz, J., Heillman, M., and Derynck, R. (1999). Inhibition of TGF-beta receptor signaling in osteoblasts leads to decreased bone remodeling and increased trabecular bone mass. Development *126*, 4267–4279.

Fleischli, J.G., Laughlin, T.J., Athanasiou, K., Lanctot, D.R., Lavery, L., Wang, X., and Agrawal, C.M. (2006). Effect of diabetes mellitus on the material properties of the distal tibia. J. Am. Podiatr. Med. Assoc. *96*, 91–95.

Fowler, T.W., Acevedo, C., Mazur, C.M., Hall-Glenn, F., Fields, A.J., Bale, H.A., Ritchie, R.O., Lotz, J.C., Vail, T.P., and Alliston, T. (2017). Glucocorticoid suppression of osteocyte perilacunar remodeling is associated with subchondral bone degeneration in osteonecrosis. Sci. Rep. *7*, 44618.

Franz-Odendaal, T.A., Hall, B.K., and Witten, P.E. (2006). Buried alive: how osteoblasts become osteocytes. Dev. Dyn. *235*, 176–190.

Grafe, I., Yang, T., Alexander, S., Homan, E., Lietman, C., Jiang, M.M., Bertin, T., Munivez, E., Chen, Y., Dawson, B., et al. (2014). Excessive TGFβ signaling is a common mechanism in Osteogenesis Imperfecta. Nat. Med. *20*, 670–675.

Graycar, J.L., Miller, D.A., Arrick, B.A., Lyons, R.M., Moses, H.L., and Derynck, R. (1989). Human transforming growth factor-beta 3: recombinant expression, purification, and biological activities in comparison with transforming growth factors-beta 1 and -beta 2. Mol. Endocrinol. *3*, 1977–1986.

Haller, A.C., and Zimny, M.L. (1977). Effects of hibernation on interradicular alveolar bone. J. Dent. Res. *56*, 1552–1557.

Halleux, C., Kramer, I., Allard, C., and Kneissel, M. (2012). Isolation of mouse osteocytes using cell fractionation for gene expression analysis. Methods Mol. Biol. *816*, 55–66.

Hernandez, C.J., and Keaveny, T.M. (2006). A biomechanical perspective on bone quality. Bone *39*, 1173–1181.

Holmbeck, K., Bianco, P., Pidoux, I., Inoue, S., Billinghurst, R.C., Wu, W., Chrysovergis, K., Yamada, S., Birkedal-Hansen, H., and Poole, A.R. (2005). The metalloproteinase MT1-MMP is required for normal development and maintenance of osteocyte processes in bone. J. Cell Sci. *118*, 147–156.

Inoue, K., Mikuni-Takagaki, Y., Oikawa, K., Itoh, T., Inada, M., Noguchi, T., Park, J.S., Onodera, T., Krane, S.M., Noda, M., and Itohara, S. (2006). A crucial role for matrix metalloproteinase 2 in osteocytic canalicular formation and bone metabolism. J. Biol. Chem. *281*, 33814–33824.

Jáuregui, E.J., Akil, O., Acevedo, C., Hall-Glenn, F., Tsai, B.S., Bale, H.A., Liebenberg, E., Humphrey, M.B., Ritchie, R.O., Lustig, L.R., and Alliston, T. (2016). Parallel mechanisms suppress cochlear bone remodeling to protect hearing. Bone *89*, 7–15.

Kaya, S., Basta-Pljakic, J., Seref-Ferlengez, Z., Majeska, R.J., Cardoso, L., Bromage, T.G., Zhang, Q., Flach, C.R., Mendelsohn, R., Yakar, S., et al. (2017). Lactation-induced changes in the volume of osteocyte lacunar-canalicular space alter mechanical properties in cortical bone tissue. J. Bone Miner. Res. *32*, 688–697.

Kinoshita, A., Saito, T., Tomita, H., Makita, Y., Yoshida, K., Ghadami, M., Yamada, K., Kondo, S., Ikegawa, S., Nishimura, G., et al. (2000). Domain-specific mutations in TGFB1 result in Camurati-Engelmann disease. Nat. Genet. *26*, 19–20.

Kogawa, M., Wijenayaka, A.R., Ormsby, R.T., Thomas, G.P., Anderson, P.H., Bonewald, L.F., Findlay, D.M., and Atkins, G.J. (2013). Sclerostin regulates release of bone mineral by osteocytes by induction of carbonic anhydrase 2. J. Bone Miner. Res. *28*, 2436–2448.

Krstic, J., and Santibanez, J.F. (2014). Transforming growth factor-beta and matrix metalloproteinases: functional interactions in tumor stroma-infiltrating myeloid cells. Sci. World J. *2014*, 521754.

Kulkarni, R.N., Bakker, A.D., Gruber, E.V., Chae, T.D., Veldkamp, J.B., Klein-Nulend, J., and Everts, V. (2012). MT1-MMP modulates the mechanosensitivity of osteocytes. Biochem. Biophys. Res. Commun. *417*, 824–829.

Lane, N.E., Yao, W., Balooch, M., Nalla, R.K., Balooch, G., Habelitz, S., Kinney, J.H., and Bonewald, L.F. (2006). Glucocorticoid-treated mice have localized

changes in trabecular bone material properties and osteocyte lacunar size that are not observed in placebo-treated or estrogen-deficient mice. J. Bone Miner. Res. *21*, 466–476.

Launey, M.E., and Ritchie, R.O. (2009). On the fracture toughness of advanced materials. Adv. Mater. *21*, 2103–2110.

Levéen, P., Larsson, J., Ehinger, M., Cilio, C.M., Sundler, M., Sjöstrand, L.J., Holmdahl, R., and Karlsson, S. (2002). Induced disruption of the transforming growth factor beta type II receptor gene in mice causes a lethal inflammatory disorder that is transplantable. Blood *100*, 560–568.

Loots, G.G., Keller, H., Leupin, O., Murugesh, D., Collette, N.M., and Genetos, D.C. (2012). TGF-β regulates sclerostin expression via the ECR5 enhancer. Bone *50*, 663–669.

Lu, Y., Xie, Y., Zhang, S., Dusevich, V., Bonewald, L.F., and Feng, J.Q. (2007). DMP1-targeted Cre expression in odontoblasts and osteocytes. J. Dent. Res. *86*, 320–325.

Mohammad, K.S., Chen, C.G., Balooch, G., Stebbins, E., McKenna, C.R., Davis, H., Niewolna, M., Peng, X.H., Nguyen, D.H., Ionova-Martin, S.S., et al. (2009). Pharmacologic inhibition of the TGF-beta type I receptor kinase has anabolic and anti-catabolic effects on bone. PLoS ONE *4*, e5275.

Nalla, R.K., Kruzic, J.J., Kinney, J.H., and Ritchie, R.O. (2004). Effect of aging on the toughness of human cortical bone: evaluation by R-curves. Bone *35*, 1240–1246.

Nguyen, J., Tang, S.Y., Nguyen, D., and Alliston, T. (2013). Load regulates bone formation and Sclerostin expression through a TGFβ-dependent mechanism. PLoS ONE *8*, e53813.

Ott, S.M. (1993). When bone mass fails to predict bone failure. Calcif. Tissue Int. *53* (*Suppl 1*), S7–S13.

Ploton, D., Menager, M., Jeannesson, P., Himber, G., Pigeon, F., and Adnet, J.J. (1986). Improvement in the staining and in the visualization of the argyrophilic proteins of the nucleolar organizer region at the optical level. Histochem. J. *18*, 5–14.

Qing, H., and Bonewald, L.F. (2009). Osteocyte remodeling of the perilacunar and pericanalicular matrix. Int. J. Oral Sci. *1*, 59–65.

Qing, H., Ardeshirpour, L., Pajevic, P.D., Dusevich, V., Jahn, K., Kato, S., Wysolmerski, J., and Bonewald, L.F. (2012). Demonstration of osteocytic perilacunar/canalicular remodeling in mice during lactation. J. Bone Miner. Res. *27*, 1018–1029.

Rivadeneira, F., and Mäkitie, O. (2016). Osteoporosis and bone mass disorders: from gene pathways to treatments. Trends Endocrinol. Metab. *27*, 262–281.

Schuit, S.C., van der Klift, M., Weel, A.E., de Laet, C.E., Burger, H., Seeman, E., Hofman, A., Uitterlinden, A.G., van Leeuwen, J.P., and Pols, H.A. (2004). Fracture incidence and association with bone mineral density in elderly men and women: the Rotterdam Study. Bone *34*, 195–202.

Seeman, E. (2008). Bone quality: the material and structural basis of bone strength. J. Bone Miner. Metab. *26*, 1–8.

Selvamurugan, N., Kwok, S., Alliston, T., Reiss, M., and Partridge, N.C. (2004). Transforming growth factor-beta 1 regulation of collagenase-3 expression in osteoblastic cells by cross-talk between the Smad and MAPK signaling pathways and their components, Smad2 and Runx2. J. Biol. Chem. *279*, 19327–19334.

Sinha, S., Nevett, C., Shuttleworth, C.A., and Kielty, C.M. (1998). Cellular and extracellular biology of the latent transforming growth factor-beta binding proteins. Matrix Biol. *17*, 529–545.

Sornay-Rendu, E., Boutroy, S., Munoz, F., and Delmas, P.D. (2007). Alterations of cortical and trabecular architecture are associated with fractures in postmenopausal women, partially independent of decreased BMD measured by DXA: the OFELY study. J. Bone Miner. Res. *22*, 425–433.

Tang, S.Y., and Alliston, T. (2013). Regulation of postnatal bone homeostasis by TGFβ. Bonekey Rep. *2*, 255.

Tang, Y., Wu, X., Lei, W., Pang, L., Wan, C., Shi, Z., Zhao, L., Nagy, T.R., Peng, X., Hu, J., et al. (2009). TGF-beta1-induced migration of bone mesenchymal stem cells couples bone resorption with formation. Nat. Med. *15*, 757–765.

Tang, S., Herber, R.P., Ho, S., and Alliston, T. (2012). Matrix metalloproteinase-13 is required for osteocytic perilacunar remodeling and maintains bone fracture resistance. J. Bone Miner. Res. *27*, 1936–1950.

Teti, A., and Zallone, A. (2009). Do osteocytes contribute to bone mineral homeostasis? Osteocytic osteolysis revisited. Bone *44*, 11–16.

Van Staa, T.P., Laan, R.F., Barton, I.P., Cohen, S., Reid, D.M., and Cooper, C. (2003). Bone density threshold and other predictors of vertebral fracture in patients receiving oral glucocorticoid therapy. Arthritis Rheum. *48*, 3224–3229.

Wysolmerski, J.J. (2013). Osteocytes remove and replace perilacunar mineral during reproductive cycles. Bone *54*, 230–236.